# Paper-Based SERS Swab for Rapid Trace Detection on Real-World Surfaces

**Chang H. Lee, Limei Tian, and Srikanth Singamaneni***

Department of Mechanical Engineering and Materials Science, Washington University, St. Louis, Missouri 63130, United States

**ABSTRACT** One of the important but often overlooked considerations in the design of surface-enhanced Raman scattering (SERS) substrates for trace detection is the efficiency of sample collection. Conventional designs based on rigid substrates such as silicon, alumina, and glass resist conformal contact with the surface under investigation, making the sample collection inefficient. We demonstrate a novel SERS substrate based on common filter paper adsorbed with gold nanorods, which allows conformal contact with real-world surfaces, thus dramatically enhancing the sample collection efficiency compared to conventional rigid substrates. We demonstrate the detection of trace amounts of analyte (140 pg spread over 4 $cm^2$) by simply swabbing the surface under investigation with the novel SERS substrate. The hierarchical fibrous structure of paper serves as a 3D vasculature for easy uptake and transport of the analytes to the electromagnetic hot spots in the paper. Simple yet highly efficient and cost-effective SERS substrate demonstrated here brings SERS-based trace detection closer to real-world applications.

**KEYWORDS:** surface-enhanced Raman scattering • paper substrates • trace detection • gold nanorods • SERS swab • paper plasmonics

Surface-enhanced Raman scattering (SERS) is emerging as a powerful technique for the trace level detection of various biological and chemical species and is believed to make a huge impact in life sciences, environmental monitoring, and homeland security (1−7). Numerous SERS substrates from roughened noble metal surfaces to e-beam patterned metal nanostructures with enhancement factors ranging from $1 \times 10^4$ to $1 \times 10^{10}$ have been demonstrated over the last two decades (6, 8−11). Very high enhancement factors (>$10^9$) have been reported for SERS substrates fabricated from top-down and bottom-up approaches such as e-beam lithography, colloidal lithography, on-wire lithography, and self- and directed-assembly, which enable precise control over the size, shape, and organization of the metal nanostructures (12−16). On the other hand, 3D SERS substrates such as photonic crystal fibers and porous alumina membranes decorated with nanoparticles and periodic nanohole arrays also offer large SERS enhancements ($1 \times 10^6$ to $1 \times 10^9$) owing to the large surface area within the source laser footprint and efficient light-matter interaction compared to the 2D counterparts (17−20).

Although most of these studies clearly demonstrate that SERS substrates hosting closely separated metal nanostructures and/or sharp tips result in large enhancements, an important practical consideration apart from the cost, which is often overlooked, is the ease and efficiency of the sample collection. In real-world applications such as explosive detection, the efficiency of sample collection becomes a decisive factor. For example, in the case of explosives such as trinitrotoluene (TNT), which inherently have low vapor pressure (~10 $ppb_v$ at room temperature), intentional packaging further lowers the actual vapor concentration by more than an order of magnitude (21). For detection of such explosives, it is extremely important to collect particulates (few $\mu$g), that are invariably present on the surface of objects exposed to the explosive. Physical swabbing, puffer systems (aerodynamic), and direct vapor sniffing are recognized as efficient methods to collect trace amounts of analytes. In particular, swabbing the surface under investigation with a soft and flexible substrate (swab) is a highly practical and efficient method to maximize the sample collection from a real-world surface. In fact, this strategy is being extensively employed for passenger screening at airports using ion mobility spectroscopy (22). On the contrary, conventional SERS substrates based on silicon, glass, and porous alumina, which are conceived for homeland security applications, are not compatible with such an efficient sample collection process because of their nonconformal, rigid, and brittle nature.

Herein, we demonstrate the fabrication of a simple yet highly efficient paper-based SERS substrate by loading gold nanorods (AuNR) in a commercially available laboratory filter paper. The SERS substrate demonstrated here can be used by simply swabbing the surface of an object suspected of exposure to a hazardous material. We demonstrate the detection of less than 140 pg of 1,4-benzenedithiol (1,4-BDT) residue spread over 4 $cm^2$ surface by swabbing the AuNR-loaded paper on the surface. Previous attempts employing filter paper exhibited limited sensitivity, possibly because of the thin metal films (thermally evaporated or sputtered) or poor control over the size and shape of the metal nanostructures employed in these designs (23, 24). Apart from the large enhancement, the uniform decoration of the nanorods demonstrated here preserves the favorable attributes such

* To whom correspondence should be addressed. E-mail: singamaneni@wustl.edu.

Received for review October 12, 2010 and accepted November 29, 2010

DOI: 10.1021/am1009875

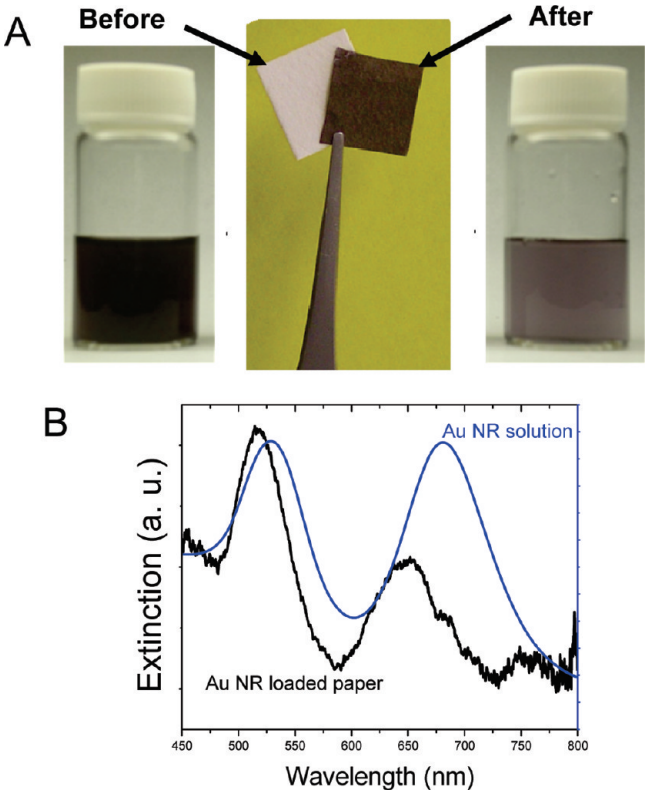


**FIGURE 1. (A) Photographs of the AuNR solutions and the filter paper before and after exposure showing the strong color change, (B) UV−vis extinction spectra of the AuNR solution and the AuNR-loaded paper showing the transverse and longitudinal plasmon absorption of the AuNR.**

as flexibility, conformal nature, and capillarity of the paper. To the best of our knowledge, this study presents the first SERS swab for rapid and efficient sample collection from real-world surfaces with unprecedented sensitivity.

Gold nanorods were synthesized using a previously reported seed-mediated approach using cetyltrimethylammonium bromide (CTAB) as a capping agent (see Experimental Section) (25, 26). The nanorods were found to be ∼80 nm long and ∼20 nm in diameter, making the aspect ratio nearly four. Exposing the filter paper to CTAB-capped gold nanorod solution resulted in uniform adsorption of the nanorods on the surface of the paper and a color change from white to purple (Figure 1A). A significant decrease in the intensity of the purple color of the AuNR solution was observed after removing the paper from the solution (see Figure 1A), which corresponded to a nearly 50% decrease in extinction intensity. This significant change in the intensity of the color of the solution following the filter paper exposure is in accordance with the high density of nanorods on the surface of the paper and deep purple color of the paper. UV−vis extinction spectra of the AuNR solution showed the two characteristic peaks at ∼530 and 650 nm corresponding to the transverse and longitudinal plasmon resonances of the nanorods, respectively (see Figure 1B) (27). AuNR-loaded paper exhibited a similar extinction spectrum with both transverse and longitudinal plasmon slightly blue-shifted compared to the solution. The observed blue shift can be attributed to the change in the dielectric ambient (from water to air + substrate) with an effective decrease in the refractive index. The blue shift of the longitudinal plasmon peak (34 nm) was found to be slightly higher compared to the transverse band (12 nm), which can be attributed to the higher sensitivity of the longitudinal plasmon resonance to the change in the dielectric ambient compared to the transverse band (28).

Cellulose is biodegradable, renewable, and abundant in nature thus cellulose (or paper) based products can be inexpensively produced and recycled (29). Because of numerous advantages such as significant reduction in cost, high specific surface area, excellent wicking property, and compatibility with conventional printing approaches (enabling multiplexed detection and easy disposability), paper is gaining increased attention as a substrate in diagnostic and tissue engineering applications (30−34). Figure 2A shows the hierarchical fibrous morphology of the filter paper with cellulose nanofibers braided into microfibers (average diameter of ∼0.4 $\mu$m). The RMS surface roughness of the paper was found to be 72 nm over 5 × 5 $\mu m^2$ area, which indicates large surface area of the paper substrates. Raman spectra obtained from six different areas of the pristine filter paper with 1 in. diameter exhibited excellent compositional (spectral) homogeneity, which is extremely important for its application as a SERS substrate (see the Supporting Information, Figure S1). It is well-known that uniform and high density adsorption of CTAB (cationic surfactant)-capped AuNR to polymer surfaces is a significant challenge (35, 36). We observed that once the AuNR-loaded paper was dried, even under vigorous rinsing with water or alcohol, no noticeable change in the AuNR density was observed, suggesting the stability of the substrate for deployment in liquid environments. Cellulose has a large number of hydroxyl groups, which are accessible for attaching positively charged species (29, 37). The uniform, irreversible, and high-density adsorption of the AuNR is possibly due to the electrostatic interaction between the positive charged nanorods and the filter paper.

AFM images revealed a uniform and dense adsorption of nanorods on the surface of the paper without any signs of large scale aggregation of the nanorods (Figure 2B). Higher-magnification AFM images show the nanorods decorating the fibers of the paper and a partial local alignment of the nanorods along the nanofibers (Figure 2C,D). From numerous AFM images collected at different areas of the substrate, the number density of the nanorods was found to be 98 ± 22/$\mu m^2$. High-magnification SEM image shows the uniformly adsorbed gold nanorods on the paper (Figure 2E). Energy-dispersive X-ray spectra (EDX) confirmed the presence of gold on the surface apart from the carbon- and oxygen-rich cellulose fibers (inset of Figure 2E).

1,4-Benzenedithiol (1,4-BDT) is widely employed as a model analyte for SERS because of its ability to readily adsorb on gold or silver particles and its distinct Raman fingerprint. The Raman spectrum of 1,4-BDT in neat solid state exhibits strong bands at 740, 1058, 1093, 1186, and 1573 $cm^{-1}$. Three prominent bands: 1058 $cm^{-1}$ due to the

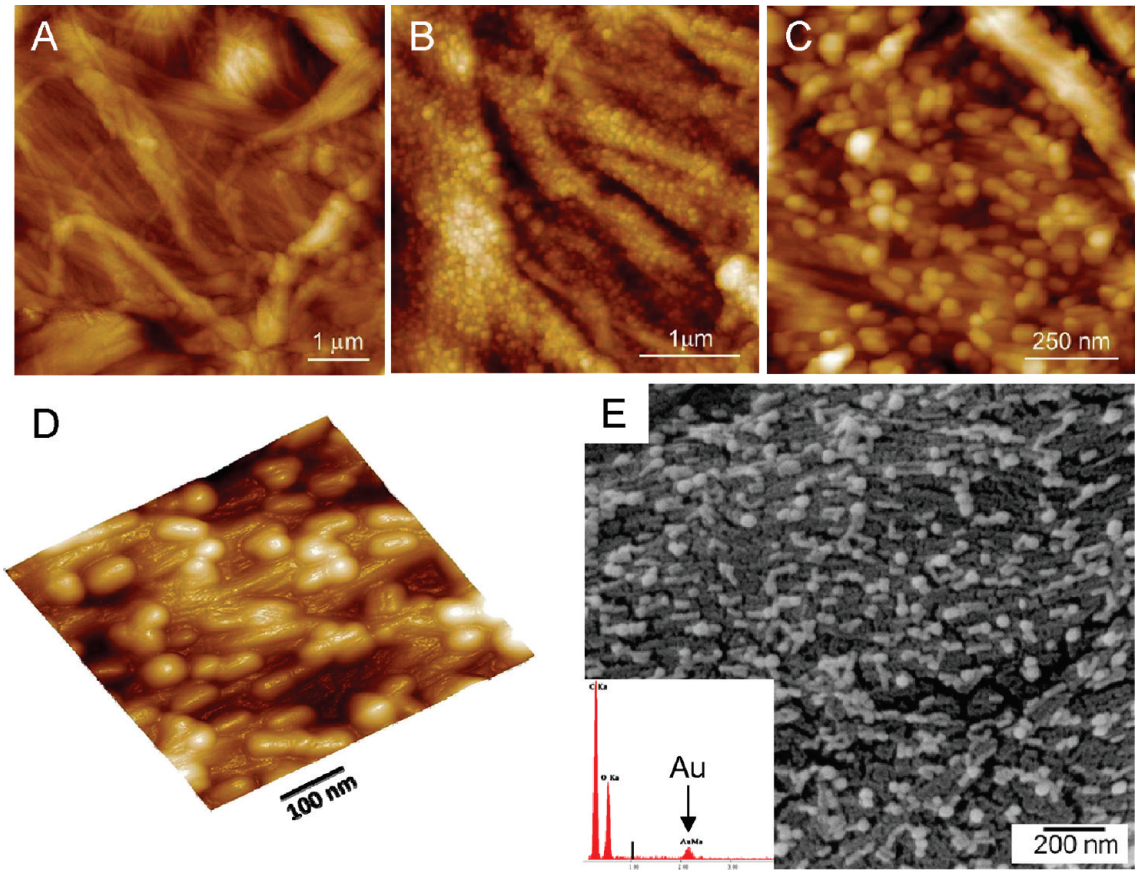


FIGURE 2. AFM images of (A) bare filter paper, (B) paper with gold nanorods, (C) higher-magnification image showing the nanorods uniformly decorating the fibers of the paper, (D) 3D AFM image showing the partial local alignment of the nanorods along the fibers, (E) SEM showing the large scale uniformity of the gold nanorods adsorbed on the surface of the paper (inset shows the EDX confirming the presence of the gold on the surface of the paper).

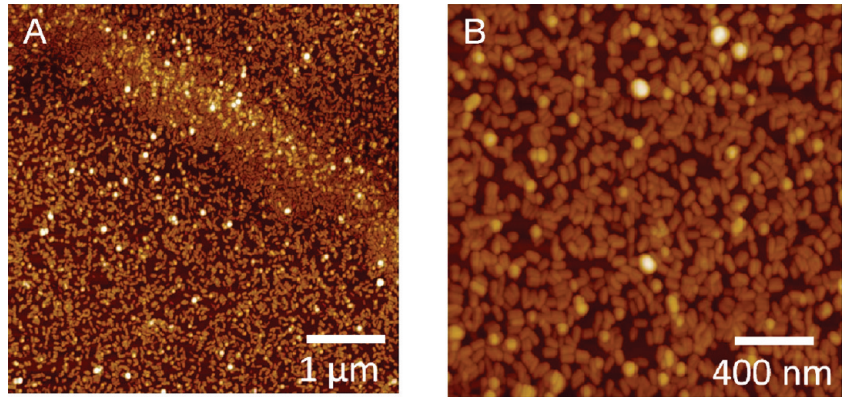


FIGURE 3. AFM images of (A) uniform and high density array of nanorods on silicon surface modified with poly(2-vinyl pyridine) and (B) higher-magnification image showing the gold nanorods shown in A.

combination of the phenyl ring breathing mode, CH in-plane bending, and CS stretching; 1181 $cm^{-1}$ due to CH bending; and 1562 $cm^{-1}$ due to phenyl ring stretching are commonly employed as characteristic peaks for evaluating the performance of SERS substrates (38−40). We utilized the 1058 $cm^{-1}$ band to test the performance of our SERS substrate in detecting trace amounts of 1,4-BDT in ethanol. The pristine SERS substrate (AuNR-loaded paper) does not show any peak in this region (see the Supporting Information, Figure S2).

As a planar rigid substrate for comparison, we employed a highly dense (number density: 220 ± 14 /$\mu m^2$) layer of gold nanorods bound to silicon substrate modified with poly(2-vinyl pyridine) (Figure 3). Figure 4A shows the Raman spectra obtained from the planar AuNR control sample and AuNR loaded paper both exposed to 1 mM of 1,4-BDT, followed by rinsing with ethanol. While the Raman spectra obtained from the AuNRs on silicon substrate exhibits weak Raman bands of 1,4-BDT, the AuNR-loaded paper exhibited much stronger (~250 times) Raman bands. These Raman spectra obtained from the SERS substrates exhibited small shifts in frequency of the vibrational bands compared to the bulk 1,4-BDT (i.e., 1185 $cm^{-1}$ for bulk BDT, and 1180 $cm^{-1}$

for SERS substrate), possibly because of the orientation change of 1,4-BDT molecules adsorbed on to the AuNR (41).

To investigate the trace detection ability of the paper based SERS substrate, Raman spectra were collected from substrates exposed to 1,4-BDT down to concentrations of 0.1 nM. All the characteristic bands of the 1,4-BDT exhibited a monotonous decrease in intensity with decreasing concentration (Figure 4B). Figure 4C shows the higher resolution spectra of the smoothed 1058 $cm^{-1}$ band, which is clearly distinguishable (signal-to-noise ratio of 3) down to a concentration of 0.1 nM (17 ppt) (the Supporting Information, Figure S3, shows higher-resolution spectra). Semilog plot of the concentration vs 1058 $cm^{-1}$ peak intensity shows a monotonic increase in the Raman intensity with increasing concentration of the analyte (Figure 4D). Data from Figure 4D can be plotted as the inverse of the fractional coverage (taken as a ratio of intensity, $I_{max}/I$) with respect to the inverse of the concentration ($1/c$), which exhibits a linear relationship, reflecting the expected Langmuir adsorption isotherm of 1,4-BDT to gold nanorods (inset of Figure 4D) (42).

The following expression was used to calculate the enhancement factor (EF) of SERS substrate at 1058 $cm^{-1}$ band

$$EF = I_{SERS} \times N_{bulk}/I_{bulk} \times N_{SERS} \quad (1)$$

where $I_{SERS}$ ($N_{SERS}$) and $I_{bulk}$ ($N_{bulk}$) are the intensities (the number of 1,4-BDT molecules probed) for the SERS and bulk spectra, respectively (41). $N_{SERS}$ was estimated by assuming a complete monolayer of 1,4-BDT on the nanorods for SERS substrates exposed to 1 mM concentration, which ensures that the enhancement factor is not overestimated. On the basis of numerous AFM images, the areal coverage of the AuNR was estimated to be ~23% and $N_{SERS}$ was calculated to be $4.9 \times 10^5$ molecules. $I_{bulk}$ and $N_{bulk}$ were determined from the Raman spectra of a 0.1 M of 1,4-BDT in 12 M $NaOH_{(aq)}$ (see Experimental Section for details). Using the SERS intensity of the 1058 $cm^{-1}$ band, the enhancement factor was calculated to be $\sim 5 \times 10^6$. The enhancement factor observed here is high considering the absence of any resonance contribution, the use of gold nanostructures as opposed to silver nanostructures, which result in higher enhancement at the expense of poor long-term stability, the absence of any intentionally formed hot spots (dimers or controlled aggregates), and the simplicity of the fabrication approach (43).

One of the distinct advantages of the paper-based SERS substrate is the ability to collect trace amount of analytes from real-world surfaces by swabbing across the surface. We

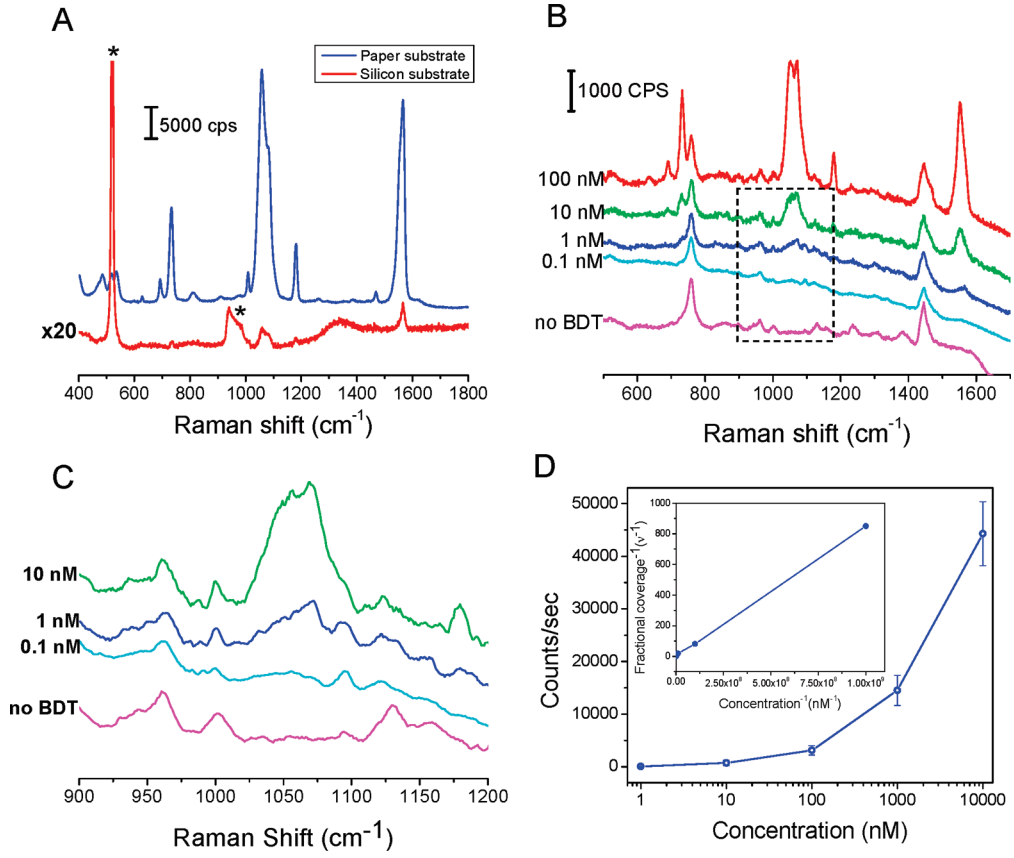


FIGURE 4. (A) Raman spectra collected from AuNR-loaded paper and 2D assembly of AuNR, both exposed to 1 mM 1,4-BDT; Raman bands indicated with asterisk (*) correspond to silicon substrate (B) SERS spectra from AuNR loaded paper exposed to different concentrations of 1,4-BDT (C) higher-resolution spectra (smoothed) showing 1058 $cm^{-1}$ band, (D) concentration vs SERS intensity plot showing a monotonous increase in SERS intensity with increasing 1,4-BDT concentration (inset shows the plot of the inverse of the fractional coverage vs inverse concentration).

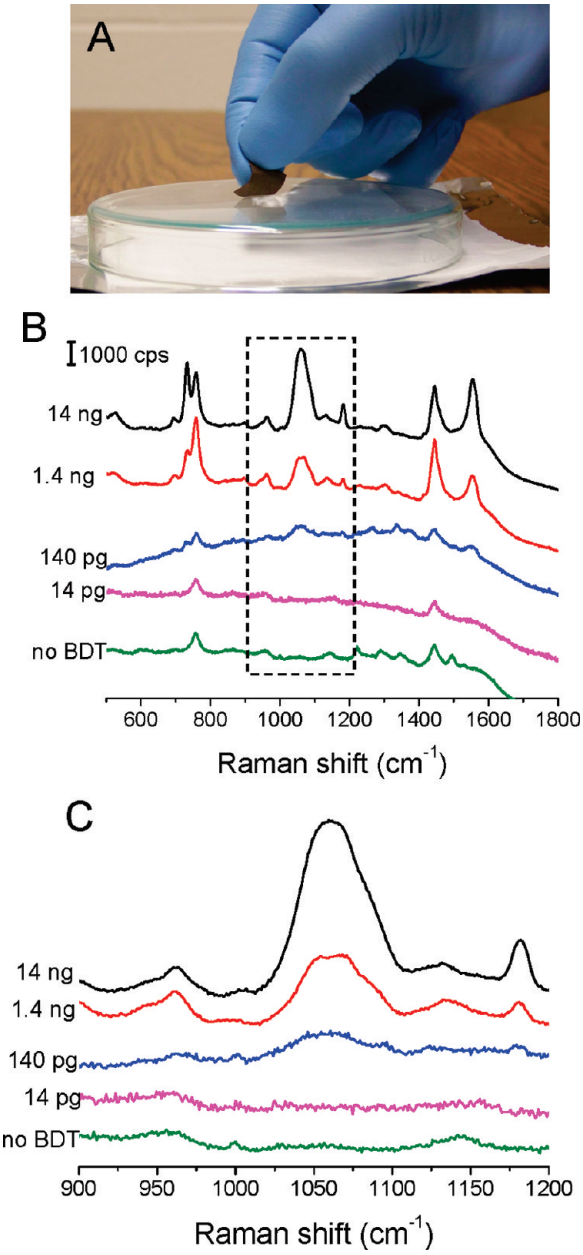


**FIGURE 5. (A) Photograph showing the SERS substrate being swabbed on the glass surface to collect trace amounts of analyte, (B) SERS spectra from AuNR loaded paper swabbed on a glass surface with different amounts of 1,4-BDT, (C) higher-resolution spectra showing the 1058 $cm^{-1}$ band.**

demonstrate this unique ability of the paper substrate by swabbing a slightly wetted (in ethanol) paper on surface of a glass with trace quantities of analyte deposited on the surface (see Figure 5A). Figure 5B shows the Raman spectra (averaged over 6 different spots) obtained by swabbing the paper across the surface with different amounts of analyte. Again, we used the strongest Raman band at 1058 $cm^{-1}$ to evaluate the efficiency of the SERS swab. It can be seen that the Raman bands of 1,4-BDT can be clearly distinguished down to 140 pg on the surface (Figure 5C). Considering that the swabbing of the surface results in only a fraction of the analyte being absorbed into the paper, a detection limit on the order of few tens of picograms on the surface is truly remarkable.

Envisioned and designed as an end-user level SERS substrate, proper handling of paper SERS substrate becomes an important issue as they contain metal nanostructures, which could be potentially harmful to humans and the environment. Toxicity of gold nanoparticles is still debated, even though many reports indicate that gold nanoparticles are essentially nontoxic. In a recent perspective, Alkilany et al. suggested that the toxicity and cell uptake of gold nanorods can be controlled to a point that they would not pose a serious harm by functionalizing the surface of gold nanorods with biocompatible ligands (44, 45). A similar approach, i.e., tailoring the surface chemistry of the metal nanostructures, can be employed to make the paper SERS substrates biofriendly.

In conclusion, we have demonstrated highly efficient SERS substrate based on common filter paper filled with gold nanorods, which exhibited more than 2 orders of magnitude higher SERS enhancement compared to the silicon-based SERS substrate. Numerous favorable traits of the paper such as flexibility, conformability, efficient uptake, and transport of the analytes from liquid and solid media to the surface of metal nanostructures due to hierarchical vasculature and high specific surface area make the paper-based SERS substrates demonstrated here an excellent candidate for trace chemical and biological detection. The paper-based SERS substrate also offer cost-effective platform for SERS detection and open up a new venue for other biological and chemical detection. The process demonstrated here can be easily scaled up for batch fabrication of SERS swabs. Furthermore, the paper-based SERS substrate introduces a novel platform for integrating conventional chromatography, microfluidics and biological assays (e.g., Western blot analysis) with SERS, imparting chemical specificity to these techniques. Similar to microfluidic devices, paper SERS-based multiplexed detection of analytes from a complex real-world sample can be a very powerful approach, which is a subject of our future investigation (46). We also see electrospinning of polymer fibers as a potential method for realizing flexible SERS substrates. Electrospun polymer mats possess a hierarchical fibrous structure similar to that of paper, and the use of different types of polymers in electrospinning can bring better control (fiber diameter, alignment, surface chemistry) and multifunctionality to the SERS design and applications.

## EXPERIMENTAL SECTION

Gold nanorods had been synthesized using a seed-mediated approach (26, 27). Seed solution was prepared by adding 1 mL of an ice-cold solution of 10 mM sodium borohydride into 10 mL of magnetically stirred 0.1 M cetyltrimethylammonium bromide (CTAB) and $2.5 \times 10^{-4}$ M $HAuCl_4$(aq) solution at room temperature. The color of the seed solution changed from yellow to brown. Growth solution was prepared by mixing 95 mL of 0.1 M CTAB, 1 mL of 10 mM silver nitrate, 5 mL of 10 mM $HAuCl_4$, and 0.55 mL of 0.1 M ascorbic acid in the same order. The solution was homogenized by gentle stirring. To the resulting colorless solution was added 0.12 mL of freshly prepared seed solution and this was set aside in dark for 14 h. The solution turned from colorless to violet brown, with most

of the color change happening in the first hour. Prior to use, the gold nanorod solution was centrifuged at 13 000 rpm for 10 min to remove excess CTAB and redispersed in nanopure water (18.2 MΩ cm). The procedure was repeated twice. AuNRs were loaded in a laboratory filter paper (Whatman No. 1 grade) by immersing a 1 $cm^2$ paper in 2.5 mL of AuNR solution for 2 days. Upon being removed from the solution, the paper was gently rinsed with nanopure water and then blow-dried under a stream of dry nitrogen. Planar silicon substrates for comparison were fabricated by modifying the silicon substrate with poly(2-vinyl pyridine) (P2VP) by exposing the piranha cleaned silicon surface to 4% P2VP solution in ethanol. After rinsing the silicon substrate with ethanol, it was exposed to gold nanorod solution to enable adsorption of the gold nanorods. Finally, the substrate was rinsed with water to remove the loosely bound nanorods, leaving a highly dense layer of nanorods on the surface.

For the dipping test, we evaluated the performance of detecting a trace amount of 1,4-BDT by dipping the SERS substrate in various concentrations of 1,4-BDT in ethanol for 20 min, followed by light rinsing with ethanol and drying with compressed nitrogen gas before the Raman measurements. Six Raman scans were performed for each substrate with each scan representing a different spot within the same substrate. The Raman data were averaged and normalized against the 1058 $cm^{-1}$ band.

For the swabbing test, 100 $\mu$L of 1 $\mu$M to 1 nM 1,4-BDT (corresponding to ~14 $\mu$g to 14 pg) in ethanol was pipetted on the surface of a glass slide, which immediately spread over 4 $cm^2$ area. Evaporation of ethanol left residue of 1,4-BDT. We placed a drop of ethanol on a 0.5 × 1 cm SERS substrate to wet, and then swabbed the surface of the glass slide to pick up the residue of 1,4-BDT. We collected Raman spectra of the swabbed SERS substrate on six different spots. The Raman spectra were averaged and normalized against the 1058 $cm^{-1}$ band.

Raman spectra were measured using a Renishaw inVia confocal Raman spectrometer mounted on a Leica microscope with 20× objective (NA = 0.40) in the range of 100 − 3200 $cm^{-1}$ with one accumulation and 10 s exposure time. A 785 nm wavelength diode laser (0.5 mW) coupled to a holographic notch filter with a grating of 1200 lines $mm^{-1}$ was used to excite the sample. The following expression was used to approximate the laser spot size (1.2 $\mu$m in diameter) (40)

$$w_0 = \frac{0.61\lambda}{\mathrm{NA}} \tag{2}$$

where $w_0$ is the minimum waist diameter for a laser beam of wavelength $\lambda$ focused by a objective with a numerical aperture NA. The focal volume ($\tau$) was approximated from the following expressions (47, 48)

$$\tau = \left(\frac{\pi}{2}\right)^{1.5} w_0^2 z_0 \tag{3}$$

$$z_0 = \frac{2\pi w_0^2}{\lambda} \tag{4}$$

where $z_0$ is the focal depth.

SEM images were obtained using a FEI Nova 2300 field emission SEM at an accelerating voltage of 10 kV. AFM images were obtained using Dimension 3000 (Digital instruments) AFM in light tapping mode. UV−vis spectra were measured using a CRAIC microspectrophotometer (QDI 302) coupled to a Leica optical microscope (DM 4000M) and a Shimadzu UV-1800 UV−vis spectrophotometer.

**Acknowledgment.** The authors thank Prof. Younan Xia and Matthew Rycenga from Biomedical Engineering at Washington University for providing access to confocal Raman microscopy system and valuable discussions. The authors acknowledge Nano Research Facility (NRF), a member of the National Nanotechnology Infrastructure Network (NNIN), for providing access to SEM facility. The work was supported by the startup funds from Washington University and a seed grant from Center for Materials Innovation at Washington University.

**Supporting Information Available:** Raman spectra of filter paper (Whatman No. 1 grade); Raman spectra of pristine filter paper and that loaded with AuNRs, both treated with 1 mM of 1,4-BDT; higher-resolution SERS spectra obtained from paper substrates exposed to 0.1 nM of 1,4-BDT and the control sample (without 1,4-BDT); Raman peak assignments for pristine Whatman No. 1 paper (PDF). This material is available free of charge via the Internet at http://pubs.acs.org/.

## REFERENCES AND NOTES

(1) Moskovits, M. *J. Raman Spectrosc.* **2005**, *36*, 485–496.
(2) Golightly, R. S.; Doering, W. E.; Natan, M. J. *ACS Nano* **2009**, *3*, 2859–2869.
(3) Homola, J. *Chem. Rev.* **2008**, *108*, 462–493.
(4) Fang, X.; Ahmad, S. R. *Appl. Phys. B: Laser Opt.* **2009**, *97*, 723–726.
(5) Hering, K.; Cialla, D.; Ackermann, K.; Dörfer, T.; Möller, R.; Schneidewind, H.; Mattheis, R.; Fritzsche, W.; Rösch, P.; Popp, J. *Anal Bioanal Chem.* **2008**, *390*, 113–124.
(6) Stewart, M. E.; Anderton, C. R.; Thompson, L. B.; Maria, J.; Gray, S. K.; Rogers, J. A.; Nuzzo, R. G. *Chem. Rev.* **2008**, *108*, 494–521.
(7) Haynes, C. L.; Van Duyne, R. P. *J. Phys. Chem. B* **2003**, *107*, 7426–7433.
(8) Ko, H.; Singamaneni, S.; Tsukruk, V. V. *Small* **2008**, *4*, 1576–1599.
(9) Camden, J. P.; Dieringer, J. A.; Zhao, J.; Van Duyne, R. P. *Acc. Chem. Res.* **2008**, *41*, 1653–1661.
(10) Anker, J. N.; Hall, W. P.; Lyandres, O.; Shah, N. C.; Zhao, J.; Van Duyne, R. P. *Nat. Mater.* **2008**, *7*, 442–453.
(11) Banholzer, M. J.; Millstone, J. E.; Qin, L.; Mirkin, C. A. *Chem. Soc. Rev.* **2008**, *37*, 885–897.
(12) Im, H.; Bantz, K. C.; Lindquist, N. C.; Haynes, C. L.; Oh, S. *Nano Lett.* **2010**, *10*, 2231–2236.
(13) McFarland, A. D.; Young, M. A.; Dieringer, J. A.; Van Duyne, R. P. *J. Phys. Chem. B* **2005**, *109*, 11279–11285.
(14) Tessier, P. M.; Velev, O. D.; Kalambur, A. T.; Lenhoff, A. M.; Rabolt, J. F.; Kaler, E. W. *Adv. Mater.* **2001**, *13*, 396–400.
(15) Tao, A.; Kim, F.; Hess, C.; Goldberger, J.; He, R.; Sun, Y.; Xia, Y.; Yang, P. *Nano Lett.* **2003**, *3*, 1229–1233.
(16) Qin, L.; Zou, S.; Xue, C.; Atkinson, A.; Schatz, G. C.; Mirkin, C. A. *Proc. Nat. Acad. Sci. U.S.A.* **2006**, *103*, 13300–13303.
(17) Brolo, A. G.; Arctander, E.; Gordon, R.; Leathem, B.; Kavanagh, K. L. *Nano Lett.* **2004**, *4*, 2015–2018.
(18) Ko, H.; Chang, S.; Tsukruk, V. V. *ACS Nano* **2009**, *3*, 181–188.
(19) Chang, S.; Ko, H.; Singamaneni, S.; Gunawidjaja, R.; Tsukruk, V. V. *Anal. Chem.* **2009**, *81*, 5740–5748.
(20) Han, Y.; Oo, M. K.; Zhu, Y.; Sukhishvili, S.; Xiao, L.; Demokan, M. S.; Jin, W.; Du, H. *Proc. Spie.* **2007**, *6767*, 67670G.
(21) Moore, D. S. *Rev. Sci. Instrum.* **2004**, *75*, 2499.
(22) Martinak, D.; Rudolph, A. Proc. IEEE 31st Annual 1997 International Conference on Security Technology, 188−189.
(23) Cabalín, L. M.; Laserna, J. *Anal. Chim. Acta* **1995**, *310*, 337–345.
(24) Wu, D.; Fang, Y. *J. Colloid Interface Sci.* **2003**, *265*, 234–238.
(25) Lee, K. S.; El-Sayed, M. A. *J. Phys. Chem. B* **2005**, *109*, 20331–20338.
(26) Gole, A.; Murphy, C. J. *Langmuir* **2008**, *24*, 266–272.
(27) El-Sayed, M. A. *Acc. Chem. Res.* **2001**, *34*, 257–264.

(28) Chen, C. -D.; Cheng, S.-F.; Chau, L.-K.; Chris Wang, C. R. *Biosens. Bioelec.* **2007**, *22*, 926–932.
(29) Samir, M. A. S. A.; Alloin, F.; Dufresne, A. *Biomacromolecules* **2005**, *6*, 612–626.
(30) Martinez, A. W.; Phillips, S. T.; Butte, M. J.; Whitesides, G. M. *Angew. Chem., Int. Ed.* **2007**, *46*, 1318–1320.
(31) Zhao, W.; van der Berg, A. *Lab Chip* **2008**, *8*, 1988–1991.
(32) Cheng, C.-M.; Martinez, A. W.; Gong, J.; Mace, C. R.; Phillips, S. T.; Carrilho, E.; Mirica, K. A.; Whitesides, G. M. *Angew. Chem., Int. Ed.* **2010**, *49*, 4771–4774.
(33) Martinez, A. W.; Phillips, S. T.; Whitesides, G. M. *Anal. Chem.* **2010**, *82*, 3–10.
(34) Derda, R.; Laromaine, A.; Mammoto, A.; Tang, S. K. Y.; Mammoto, T.; Ingber, D. E.; Whitesides, G. M. *Proc. Natl. Acad. Sci. U.S.A.* **2009**, *106*, 18457–18462.
(35) Koo, H. Y.; Choi, W. S.; Kim, D.-Y. *Small* **2008**, *4*, 742–745.
(36) Rutland, M. W.; Parker, J. L. *Langmuir* **1994**, *10*, 1110–1121.
(37) Habibi, Y.; Lucia, L. A.; Rojas, O. J. *Chem. Rev.* **2010**, *110*, 3479–3500.
(38) Cho, S. H.; Han, H. S.; Jang, D.-J.; Kim, K.; Kim, M. S. *J. Phys. Chem.* **1995**, *99*, 10594–10599.
(39) Joo, S. W.; Han, S. W.; Kim, K. *J. Colloid Interface Sci.* **2001**, *240*, 391–399.
(40) Camargo, P. H. C.; Cobley, C. M.; Rycenga, M.; Xia, Y. *Nanotechnology* **2009**, *20*, 434020.
(41) Chen, T.; Wang, H.; Chen, G.; Wang, Y.; Feng, Y.; Teo, W. S.; Wu, T.; Chen, H. *ACS Nano* **2010**, *4*, 3087–3094.
(42) Lee, Y. J.; Jeon, I. C.; Paik, W.; Kim, K. *Langmuir* **1996**, *12*, 5830–5837.
(43) Kelly, K. L.; Coronado, E.; Zhao, L. L.; Schatz, G. C. *J. Phys. Chem. B* **2002**, *107*, 668–677.
(44) Alkilany, A. M.; Murphy, C. J. *J. Nanopart. Res.* **2010**, *12*, 2313–2333.
(45) Takahashi, H.; Niidome, Y.; Niidome, T.; Kaneko, K.; Kawasaki, H.; Yamada, S. *Langmuir* **2006**, *22*, 2–5.
(46) Martinez, A. W.; Phillips, S. T.; Whitesides, G. M. *Proc. Natl. Acad. Sci. U.S.A.* **2008**, *105*, 19606–19611.
(47) Bridges, T. E.; Houlne, M. P.; Harris, J. M. *Anal. Chem.* **2004**, *76*, 576–584.
(48) Rüttinger, S.; Buschmann, V.; Krämer, B.; Erdmann, R.; Macdonald, R.; Koberling, F. Determination of the confocal volume for quantitative fluorescence correlation spectroscopy. In *Proceedings of SPIE-OSA Biomedical Optics*; Munich, Germany, June 17, 2007; Optical Society of America: Washington, D.C., 2007; Vol. 6630, 6630_12.

AM1009875